Inorg. Chem. **2003**, *42*, 750–760

Binuclear Manganese Compounds of Potential Biological Significance. 1. Syntheses and Structural, Magnetic, and Electrochemical Properties of Dimanganese(II) and -(II,III) Complexes of a Bridging Unsymmetrical Phenolate Ligand

Lionel Dubois,[†] Dao-Feng Xiang,[‡] Xian-Shi Tan,[‡] Jacques Pécaut,[‡] Peter Jones,[‡] Stéphane Baudron,[‡] Laurent Le Pape,[†] Jean-Marc Latour,*[,†] Carole Baffert,[§] Sylvie Chardon-Noblat,[§] Marie-Noëlle Collomb,[§] and Alain Deronzier[§]

Laboratoire de Physicochimie des Métaux en Biologie, FRE 2427, CEA-CNRS-UJF, Département Réponse et Dynamique Cellulaires, CEA-Grenoble, 38054 Grenoble Cedex 9, France, Laboratoire de Chimie Inorganique et Biologique, UMR 5046 CEA-CNRS-UJF, Département de Recherche Fondamentale sur la Matière Condensée, CEA-Grenoble, 38054 Grenoble Cedex 9, France, and Laboratoire d'Électrochimie Organique et de Photochimie Rédox, UMR CNRS 5630, Université Joseph Fourier Grenoble 1, BP 53, 38041 Grenoble Cedex 9, France

Received May 20, 2002

Reactions of the unsymmetrical phenol ligand 2-(bis(2-pyridylmethyl)aminomethyl)-6-((2-pyridylmethyl)(benzyl)-aminomethyl)-4-methylphenol with $Mn(OAc)_2 \cdot 4H_2O$ or $Mn(H_2O)_6(ClO_4)_2$ in the presence of NaOBz affords the dimanganese(II) complexes **1**(CH_3OH), $[Mn_2(L)(OAc)_2(CH_3OH)](ClO_4)$, and **2**($H_2O$), $[Mn_2(L)(OBz)_2(H_2O)](ClO_4)$, respectively. On the other hand, reaction of the ligand with hydrated manganese(III) acetate furnishes the mixed-valent derivative **3**(H_2O), $[Mn_2(L)(OAc)_2(H_2O)](ClO_4)_2$. The three complexes have been characterized by X-ray crystallography. **1**(CH_3OH) crystallizes in the monoclinic system, space group $P2_1/c$, with $a = 10.9215(6)$ Å, $b = 20.2318(12)$ Å, $c = 19.1354(12)$ Å, $\alpha = 90°$, $\beta = 97.5310(10)°$, $\gamma = 90°$, $V = 4191.7$ Å^3, and $Z = 4$. **2**(H_2O) crystallizes in the monoclinic system, space group $P2_1/n$, with $a = 10.9215(6)$ Å, $b = 20.2318(12)$ Å, $c = 19.1354(12)$ Å, $\alpha = 90°$, $\beta = 97.5310(10)°$, $\gamma = 90°$, $V = 4191.7$ Å^3, and $Z = 4$. **3**(H_2O) crystallizes in the monoclinic system, space group $P2_1/c$, with $a = 11.144(6)$ Å, $b = 18.737(10)$ Å, $c = 23.949(13)$ Å, $\alpha = 90°$, $\beta = 95.910(10)°$, $\gamma = 90°$, $V = 4974(5)$ Å^3, and $Z = 4$. Magnetic measurements revealed that the three compounds exhibit very similar magnetic exchange interactions $-J = 4.3(3)$ cm^{-1}. They were used to establish tentative magneto–structural correlations which show that for the dimanganese(II) complexes $-J$ decreases when the $Mn-O_{phenoxo}$ distance increases as expected from orbital overlap considerations. For the dimanganese(II,III) complexes, crystallographic results show that the $Mn^{II}-O_{phenoxo}$ and $Mn^{III}-O_{phenoxo}$ bond lengths are inversely correlated. An interesting magneto–structural correlation is found between $-J$ and the difference between these bond lengths, $\delta_{Mn-O} = d_{Mn^{II}-O} - d_{Mn^{III}-O}$: the smaller this difference, the larger $-J$. Electrochemical studies show that the mixed-valence state is favored in **1**–**3** by ca. 100 mV with respect to analogous complexes of symmetrical ligands, owing to the asymmetry of the electron density as found in the analogous diiron complexes.

Introduction

Numerous manganese enzymes with a dinuclear active site have been found in the recent past,[1−3] and crystal structure determinations have revealed a few features common to this class of proteins. Indeed, in the reduced state of these enzymes, the two Mn^{II} ions are bridged by a carboxylate group from a glutamate/aspartate residue and (at least) one solvent-derived oxygen bridge. One histidine nitrogen and

* To whom correspondence should be addressed. E-mail: jlatour@cea.fr.
[†] Département Réponse et Dynamique Cellulaires, CEA-Grenoble.
[‡] Département de Recherche Fondamentale sur la Matière Condensée, CEA-Grenoble.
[§] Université Joseph Fourier Grenoble 1.

(1) Dismukes, G. C. *Chem. Rev.* **1996**, *96*, 2909−2926.
(2) Christianson, D. W. *Prog. Biophys. Mol. Biol.* **1997**, *67*, 217−252.
(3) Jedrzejas, M. J.; Setlow, P. *Chem. Rev.* **2001**, *101*, 607−618.

10.1021/ic020354m CCC: $25.00
Published on Web 01/03/2003

two carboxylato oxygens from aspartate or glutamate residues usually complete the Mn^{II} coordination sphere. Most of these enzymes are hydrolases, the prototype of which is arginase involved in L-arginine hydrolysis into L-ornithine and urea.[4] A few other dimanganese enzymes have been structurally characterized, proline-specific aminopeptidase,[5] phosphoglycerate mutase,[6,7] bacteriophage λ phosphoprotein phosphatase[8] and Tn*5* transposase synaptic complex,[9] while others, such as D-xylose isomerase[10] and dinitrogenase reductase-activating glycohydrolase,[11] have been proposed to belong to this family from the observation of an EPR spectrum characteristic of a pair of weakly magnetically interacting Mn^{II} ions. Manganese has been proposed as the active metal in a bacterial ribonucleotide reductase[12] and the purple acid phosphatase from sweet potato,[13] but this was later shown to be probably false.[14,15] In both cases as in several hydrolases,[3] it is likely that Mn replacement of the active metals occurred during extraction and purification of the enzymes. In this respect, it is worth noting that Mn substitution has been used as a common tool to investigate the structural and physical properties of several proteins with a dinuclear active site such as concanavalin,[16] phosphotriesterase,[17] lobster enolase,[18] hemerythrin,[19] and ribonucleotide reductase.[20,21]

Apart from these Mn hydrolases, a few redox active Mn catalases have been found in several bacteria *Lactobacillus plantarum*,[22] *Thermus thermophilus*,[23] *Thermoleophilum album*,[24] and *Thermus* sp. YS 8−13,[25] where they catalyze hydrogen peroxide disproportionation to dioxygen and water. The recent crystal structure determinations of the Mn-catalases from *T. thermophilus*[26] and *L. plantarum*[27] have shown that these enzymes bear a strong structural analogy with arginase although they possess two solvent-derived bridges (hydroxide or water, instead of a single one) the nature of which is yet to be ascertained. Although the X-ray structures of the *T. thermophilus* and *L. plantarum* enzymes have been solved, their mechanism of action is still poorly understood. Using X-ray absorption experiments, Penner-Hahn[28] showed that during catalysis the *L. plantarum* enzyme shuttles between the $Mn^{II}{}_2$ and the $Mn^{III}{}_2$ states, but the structure of the active species is not known with certainty and no intermediate has ever been observed. Owing to the intrinsic chemical interest of H_2O_2 disproportionation reaction and the paucity of mechanistic information, the design of potentially biomimetic systems has attracted many groups.[29] This has led to the synthesis of dimanganese(II) complexes with different bridging patterns including carboxylates alone[30−34] or associated with aqua,[35−38] hydroxo,[39] alkoxo,[40,41] or phenoxo bridges.[42−50] A bis(μ-hydroxo) compound has been described also.[51] Conversely, mixed-valent $Mn^{II}Mn^{III}$

(4) Ash, D. E.; Cox, J. D.; Christianson, D. W. *Met. Ions Biol. Syst.* **2000**, *37*, 408−428.
(5) Wilce, M. C. J.; Bond, C. S.; Dixon, N. E.; Freeman, H. C.; Guss, J. M.; Lilley, P. E.; Wilce, J. A. *Proc. Natl. Acad. Sci. U.S.A.* **1998**, *95*, 3472−3477.
(6) Jedrzejas, M. J.; Chander, M.; Setlow, P.; Krishnasamy, G. *EMBO J.* **2000**, *19*, 1419−1431.
(7) Jedrzejas, M. J.; Chander, M.; Setlow, P.; Krishnasamy, G. *J. Biol. Chem.* **2000**, *275*, 23146−23153.
(8) Voegtli, W. C.; White, D. J.; Reiter, N. J.; Rusnak, F.; Rosenzweig, A. C. *Biochemistry* **2000**, *39*, 15365−15374.
(9) Lovell, S.; Goryshin, I. Y.; Reznikoff, W. B.; Rayment, I. *Nat. Struct. Biol.* **2002**, *9*, 278−281.
(10) Carrell, H. L.; Glusker, J. P.; Burger, V.; Manfre, F.; Tristsch, D.; Biellmann, J. F. *Proc. Natl. Acad. Sci. U.S.A.* **1989**, *86*, 4440−4444.
(11) Antharavally, B. S.; Poyner, R. R.; Ludden, P. W. *J. Am. Chem. Soc.* **1998**, *120*, 8897−8898.
(12) Willing, A.; Follmann, H.; Auling, G. *Eur. J. Biochem.* **1988**, *170*, 603−611.
(13) Sugiura, Y.; Kawabe, H.; Tanaka, H.; Fujimoto, S.; Ohara, A. *J. Biol. Chem.* **1981**, *256*, 10664−10670.
(14) Fieschi, F.; Torrents, E.; Toulokhonova, L.; Jordan, A.; Hellman, U.; Barbe, J.; Gibert, I.; Karlsson, M.; Sjöberg, B. M. *J. Biol. Chem.* **1998**, *273*, 4329−4337.
(15) Durmus, A.; Eicken, C.; Sift, B. H.; Kratel, A.; Kappl, R.; Huttermann, J.; Krebs, B. *Eur. J. Biochem.* **1999**, *260*, 709−716.
(16) Antanaitis, B. C.; Brown, R. D., III; Chasteen, N. D.; Freedman, J. H.; Koenig, S. H.; Lilienthal, H. R.; Peisach, J.; Brewer, C. F. *Biochemistry* **1987**, *26*, 7932−7937.
(17) Benning, M. M.; Shim, H.; Raushel, F. M.; Holden, H. M. *Biochemistry* **2001**, *40*, 2712−2722.
(18) Duquerroy, S.; Camus, C.; Janin, J. *Biochemistry* **1995**, *34*, 12513−12523.
(19) Zhang, J. H.; Kurtz, D. M. *Proc. Natl. Acad. Sci. U.S.A.* **1992**, *89*, 7065−7069.
(20) Atta, M.; Nordlund, P.; Aberg, A.; Eklund, H.; Fontecave, M. *J. Biol. Chem.* **1992**, *267*, 20682−20688.
(21) Högbom, M.; Andersson, M. E.; Nordlund, P. *JBIC* **2001**, *6*, 315−323.
(22) Kono, Y.; Fridovich, I. *J. Biol. Chem.* **1983**, *258*, 6015−6019.
(23) Barynin, V. V.; Grebenko, A. I. *Dokl. Akad. Nauk SSSR* **1986**, *286*, 461−464.
(24) Allgood, G. S.; Perry, J. J. *J. Bacteriol.* **1986**, *168*, 563−567.
(25) Mizobata, T.; Kagawa, M.; Murakoshi, N.; Kusaka, E.; Kameo, K.; Kawata, Y.; Nagai, J. *Eur. J. Biochem.* **2000**, *267*, 4264−4271.
(26) Antonyuk, S. V.; Melik-Adamyan, V. R.; Popov, A. N.; Lamzin, V. S.; Hempstead, P. D.; Harrison, P. M.; Artymyuk, P. J.; Barynin, V. V. *Cryst. Rep.* **2000**, *45*, 105−116.
(27) Barynin, V. V.; Whittaker, M. M.; Antonyuk, S. V.; Lamzin, V. S.; Harrison, P. M.; Artymiuk, P. J.; Whittaker, J. W. *Structure* **2001**, *9*, 725−738.
(28) Waldo, G. S.; Penner-Hahn, J. E. *Biochemistry* **1995**, *34*, 1507−1512.
(29) Pecoraro, V. L.; Baldwin, M. J.; Gelasco, A. *Chem. Rev.* **1994**, *94*, 807−826.
(30) Adams, H.; Bailey, N. A.; Debaecker, N.; Fenton, D. E.; Kanda, W.; Latour, J. M. *Angew. Chem., Int. Ed. Engl.* **1995**, *34*, 2535−2537.
(31) Chen, X. M.; Tong, Y. X.; Xu, Z. T.; Mak, T. C. W. *J. Chem. Soc., Dalton Trans.* **1995**, 4001−4004.
(32) Oshio, H.; Ino, E.; Mogi, I.; Ito, T. *Inorg. Chem.* **1993**, *32*, 5697−5703.
(33) Albela, B.; Corbella, M.; Ribas, J.; Castro, I.; Sletten, J.; Stoeckli-Evans, H. *Inorg. Chem.* **1998**, *37*, 788−798.
(34) Iikura, H.; Nagata, T. *Inorg. Chem.* **1998**, *37*, 4702−4711.
(35) Caneschi, A.; Ferraro, F.; Gatteschi, D.; Melandri, M. C.; Rey, P.; Sessoli, R. *Angew. Chem., Int. Ed. Engl.* **1989**, *28*, 1365−1367.
(36) Yu, S. B.; Lippard, S. J.; Shweky, I.; Bino, A. *Inorg. Chem.* **1992**, *31*, 3502−3504.
(37) Coucouvanis, D.; Reynolds, R. A., III; Dunham, W. R. *J. Am. Chem. Soc.* **1995**, *117*, 7570−7571.
(38) Ye, B. H.; Mak, T.; Williams, I. D.; Li, X. Y. *J. Chem. Soc., Chem. Commun.* **1997**, 1813−1814.
(39) Bossek, U.; Wieghardt, K. *Inorg. Chim. Acta* **1989**, *165*, 123−129.
(40) Pessiki, P. J.; Dismukes, G. C. *J. Am. Chem. Soc.* **1994**, *116*, 898−903.
(41) Boelrijk, A. E. M.; Khangulov, S. V.; Dismukes, G. C. *Inorg. Chem.* **2000**, *39*, 3009−3019.
(42) Suzuki, M.; Mirukiya, M.; Murata, S.; Uehara, A.; Oshio, H.; Kida, S.; Saito, K. *Bull. Chem. Soc. Jpn.* **1987**, *60*, 4305−4312.
(43) Mikuriya, M.; Fuji, T.; Kamisawa, S.; Kawasaki, Y.; Tokii, T.; Oshi, H. *Chem. Lett.* **1990**, 1181−1184.
(44) Gultneh, Y.; Farooq, A.; Liu, S.; Karlin, K. D.; Zubieta, J. *Inorg. Chem.* **1992**, *31*, 3606−3611.
(45) Sakiyama, H.; Tamaki, H.; Kodera, M.; Matsumoto, N.; Okawa, H. *J. Chem. Soc., Dalton Trans.* **1993**, 591−595.
(46) Mikuriya, M.; Fujii, T.; Tokii, T.; Kawamori, A. *Bull. Chem. Soc. Jpn.* **1993**, *66*, 1675−1686.
(47) Higuchi, C.; Sakiyama, H.; Okawa, H.; Isobe, R.; Fenton, D. E. *J. Chem. Soc., Dalton Trans.* **1994**, 1097−1103.
(48) Higuchi, C.; Sakiyama, H.; Okawa, H.; Fenton, D. E. *J. Chem. Soc., Dalton Trans.* **1995**, 4015−4020.

Chart 1

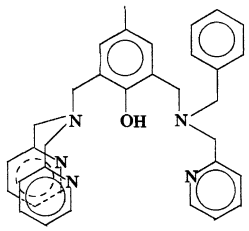

derivatives have received much less attention.[42,46,52−54] This is probably due to the fact that this redox form is not supposed to be active albeit it is present in the as-isolated Mn catalase.[55]

In this article, we report the syntheses, the X-ray structural characterization, and the physicochemical properties of dimanganese(II) and -(II,III) complexes of the hexadentate phenol-based ligand HL (Chart 1). This ligand, which was previously used to model *semi-met* hemerythrin forms,[56] combines a phenolate group to bridge the two metals and a nonbonding benzyl group which does not saturate the coordination sphere of one metal of the pair thus allowing the dimetal center to interact with a substrate without losing its integrity. Upon reaction of the ligand with Mn^{2+} salts in the presence of acetate or benzoate, the dimanganese(II) complexes $[Mn_2(L)(OAc)_2(CH_3OH)](ClO_4)$, **1**$(CH_3OH)$, and $[Mn_2(L)(OBz)_2(H_2O)](ClO_4)$, **2**$(H_2O)$, were obtained, respectively. When the same reaction was done with Mn^{3+}, the mixed-valent complex $[Mn_2(L)(OAc)_2(H_2O)](ClO_4)_2$, **3**$(H_2O)$, was obtained instead.

Experimental Section

All solvents and reagents were of the highest quality available and were used as received unless noted otherwise. The ligand HL was prepared as already reported.[57]

Syntheses.

$[Mn_2(L)(OAc)_2(CH_3OH)](ClO_4)$, 1$(CH_3OH)$. A 134 mg (0.253 mmol) amount of ligand HL was dissolved in 10 mL of methanol under argon. To this solution was added 125 mg (0.510 mmol) of $Mn(OAc)_2\cdot 4H_2O$ in 5 mL of methanol. After being stirred for 1 h, the reaction mixture was filtered and a solution of 120 mg (0.984 mmol) of sodium perchlorate was added to the filtrate. After 24 h, yellow crystals of **1**(CH_3OH) had formed; they were filtered out, washed with methanol and diethyl ether, and dried. A 135 mg (yield 50%) amount of the desired compound was obtained. Mass spectrometry (+ESI-MS): m/z $[\mathbf{1} - ClO_4]^+ = 756$. Anal. Calcd for $[Mn_2(L)(OAc)_2(OH_2)](ClO_4)\cdot H_2O$, **1**$(H_2O)\cdot H_2O$, $C_{38}H_{44}N_5O_{11}ClMn_2$: C, 51.16; H, 4.97; N, 7.85; Mn, 12.32. Found: C, 51.2; H, 5.1; N, 7.6; Mn, 11.8.

$[Mn_2(L)(OBz)_2(H_2O)](ClO_4)$, 2$(H_2O)$. A 100 mg (0.189 mmol) amount of ligand HL and 54.8 mg (0.381 mmol) of sodium benzoate were dissolved in 10 mL of methanol under argon. To this solution were added 68.8 mg (0.381 mmol) of $Mn(H_2O)_6(ClO_4)_2$ in 10 mL of methanol. The reaction mixture was filtered immediately, and after 30 mn a finely crystallized off-white solid appeared. After 24 h the solution was filtered and the crystals were washed with methanol and diethyl ether and dried. A 70 mg (yield 40%) amount of small white crystals was obtained. Mass spectrometry (+ESI-MS): m/z $[\mathbf{2} - ClO_4]^+ = 880$. Anal. Calcd for $[Mn_2(L)(OBz)_2(OH_2)](ClO_4)\cdot 2H_2O$, **2**$(H_2O)\cdot 2H_2O$, $C_{48}H_{50}N_5O_{12}ClMn_2$: C, 55.74; H, 4.87; N, 6.77; Mn, 10.62. Found: C, 55.2; H, 4.7; N, 6.8; Mn, 10.1.

$[Mn_2(L)(OAc)_2(H_2O)](ClO_4)_2$, 3$(H_2O)$. A 200 mg (0.378 mmol) amount of ligand HL was dissolved in 5 mL of methanol under argon. To this solution was added 210 mg (0.783 mmol) of hydrated manganese(III) acetate suspended in a mixture of 10 mL of methanol and 1 mL of water. After the mixture was stirred for 1 h, a solution of 150 mg (1.22 mmol) of sodium perchlorate in 5 mL of methanol was added. The reaction mixture was filtered and the filtrate left for 48 h. Dark parallelepipedic crystals of **3**(H_2O) formed which were filtered out, washed with methanol and diethyl ether, and dried. A 130 mg (yield 40%) amount of dark brown crystals was obtained. Mass spectrometry: +ESI-MS, m/z $[\mathbf{3} - 2ClO_4]^+ = 756$; −ESI-MS, m/z $[\mathbf{3} + ClO_4]^- = 1053$. Anal. Calcd for $[Mn_2(L)(OAc)_2(OH_2)](ClO_4)_2\cdot 4H_2O$, **3**$(H_2O)\cdot 4H_2O$, $C_{38}H_{52}N_5O_{19}Cl_2Mn_2$: C, 43.65; H, 4.81; N, 6.70; Mn, 10.52. Found: C, 43.5; H, 4.3; N, 6.6; Mn, 10.3.

Caution! Perchlorate salts of metal complexes with organic ligands are potentially explosive.

X-ray Crystallography. All diffraction data were taken using a Bruker SMART CCD area detector three-circle diffractometer (Mo Kα radiation, graphite monochromator, $\lambda = 0.710\ 73$ Å). Data collection for all compounds was performed at room temperature.

The cell parameters were obtained with intensities detected on three batches of 15 frames with a 5, 60, and 300 s exposure time for **1**(CH_3OH), **2**(H_2O), and **3**(H_2O), respectively. The crystal−detector distance was 5 cm. For three settings of Φ and 2Θ, 1271 narrow data frames were collected for 0.3° increments in ω with a 30, 180, and 300 s exposure time for **1**(CH_3OH), **2**(H_2O), and **3**(H_2O), respectively. A full hemisphere of data was collected for each complex. At the end of data collection, the first 50 frames were recollected to establish that crystal decay had not taken place during the collection. Unique intensities with $I > 10\sigma(I)$ detected on all frames using the SAINT program[58] were used to refine the values of the cell parameters. The substantial redundancy in data allows empirical absorption corrections to be applied using multiple measurements of equivalent reflections with the SADABS Bruker program.[58] Space groups were determined from systematic absences, and they were confirmed by the successful solution of the structure (see Table 1). Complete information on crystal data and data collection parameters is given in the Supporting Information.

The structures were solved by direct methods using the SHELXTL 5.03 package,[59] and all atoms were found by difference Fourier

(49) Aono, T.; Wada, H.; Yonemura, M.; Ohba, M.; Okawa, H.; Fenton, D. E. *J. Chem. Soc., Dalton Trans.* **1997**, 1527−1531.
(50) Sakiyama, H.; Sugawara, A.; Sakamoto, M.; Unoura, K.; Inoue, K.; Yamasaki, M. *Inorg. Chim. Acta* **2000**, *310*, 163−168.
(51) Kitajima, N.; Singh, U.; Amagai, H.; Osawa, M.; Moro-oka, Y. *J. Am. Chem. Soc.* **1991**, *113*, 7757−7758.
(52) Chang, H. R.; Diril, H.; Nilges, M. J.; Zhang, X.; Potenza, J. A.; Schugar, H. J.; Hendrickson, D. N.; Isied, S. S. *J. Am. Chem. Soc.* **1988**, *110*, 625−627.
(53) Diril, H.; Chang, H. R.; Nilges, M. J.; Zhang, X.; Potenza, J. A.; Schugar, H. J.; Isied, S. S.; Hendrickson, D. N. *J. Am. Chem. Soc.* **1989**, *111*, 5102−5114.
(54) Karsten, P.; Neves, A.; Bortoluzzi, A.; Strähle, J.; Maichle-Mössmer, C. *Inorg. Chem. Commun.* **2002**, *5*, 434−438.
(55) Michaud-Soret, I.; Jacquamet, L.; Debaecker-Petit, N.; Le Pape, L.; Barynin, V. V.; Latour, J. M. *Inorg. Chem.* **1998**, *37*, 3874−3876.
(56) Kanda, W.; Moneta, W.; Bardet, M.; Bernard, E.; Debaecker, N.; Laugier, J.; Bousseksou, A.; Chardon-Noblat, S.; Latour, J. M. *Angew. Chem., Int. Ed. Engl.* **1995**, *34*, 588−590.
(57) Lambert, E.; Chabut, B.; Chardon-Noblat, S.; Deronzier, A.; Chottard, G.; Bousseksou, A.; Tuchagues, J. P.; Bardet, M.; Laugier, J.; Latour, J. M. *J. Am. Chem. Soc.* **1997**, *119*, 9424−9437.
(58) *Software package for use with the SMART diffractometer*; Siemens Analytical X-ray Instruments Inc.: Madison, WI, 1995.

Table 1. Crystallographic Data for Complexes **1**−**3**

	1(CH_3OH)	**2**(H_2O)	**3**(H_2O)
formula	$C_{39}H_{44}N_5O_{10}ClMn_2$	$C_{48}H_{46}N_5O_{10}ClMn_2$	$C_{38}H_{42}N_5O_{14}Cl_2Mn_2$
M	896.13	1012.21	991.56
space group	$P2_1/c$	$P2_1/n$	$P2_1/c$
a (Å)	10.9215(6)	11.144(6)	21.305(2)
b (Å)	20.2318(12)	18.737(10)	10.9625(11)
c (Å)	19.1354(12)	23.949(13)	20.603(2)
β (deg)	97.5310(10)	95.910	115.837(2)
Z	4	4	4
V (Å^3)	4191.7(4)	4974(5)	4331.0(8)
ρ_{calc} (Mg·m^{-3})	1.420	1.352	1.521
T (K)	293	293	293
no. of reflcns	27 002	32 482	19 036
no. of indpt reflcns [$I > 2\sigma(I)$]	10 220	12 314	9690
no. of params	557	604	792
GOF (on F^2)	0.974	0.874	0.894
R (R_w)	0.0430 (0.1224)	0.1097 (0.2236)	0.0470 (0.0897)

syntheses. All non-hydrogen atoms were anisotropically refined on F^2. Hydrogen atoms were included in calculated positions for **1**(CH_3OH) and **2**(H_2O) and refined isotropically for **3**(H_2O).

Spectroscopy. Electronic absorption spectra were recorded on a Hewlett-Packard HP 89090A or Hewlett-Packard 8452A diode array spectrophotometer. Initial and electrolyzed solutions were transferred to a conventional cuvette cell within a glovebox. The cell was inserted into an optical translator connected to the spectrophotometer through an optical fiber system (Photonetics Spectrofip System). The optical fibers pass through the wall of the drybox via seals.

Infrared spectra were recorded with a FTIR Perkin-Elmer 1600 spectrometer, with a 1−1.5 wt % dispersion of the compound in KBr. EPR spectra were recorded on an X-band Bruker EMX spectrometer equipped with an Oxford Instruments ESR-900 continuous-flow helium cryostat and an ER-4116 DM Bruker cavity. ^{1}H and ^{13}C NMR spectra were recorded on a Bruker AC 200 spectrometer with a characteristic absorption of the solvent ($CDCl_3$, CD_3CN, or CD_3OD) as internal reference. Electrospray mass spectra were obtained with a LCQ Finnigan Thermoquest ESI source spectrometer with an ion trap and an octupolar analyzer. FAB mass spectra were obtained with a VG-ZAB-SEQ spectrometer equipped with a 35 kV Cs gun with an acceleration potential of 8 kV.

Magnetic Measurements. The overall magnetic moment M of compounds **1**−**3** was measured over the temperature range 5−300 K at 0.5 and 5 T on a Quantum Design MPMS (**1** and **3**) or a SHE 700 (**2**) superconducting quantum interference device (SQUID) magnetometer. The samples (**1**, 58 mg; **2**, 7.3 mg; **3**, 55 mg) were contained in a Kel F bucket which had been independently calibrated. The data were corrected from diamagnetism (**1**, -506×10^{-6} cm^3·mol^{-1}; **2**, -531×10^{-6} cm^3·mol^{-1}; **3**, -516×10^{-6} cm^3·mol^{-1}) using Pascal's constants.[60] The data have been simulated using the Van Vleck equations derived from the Hamiltonian $\mathscr{H} = -2J\hat{S}_1\cdot\hat{S}_2 + \beta_e\vec{H}\cdot\tilde{g}\cdot\hat{S}$.[60] Equation 1 was used for **1**(CH_3OH) and **2**(H_2O), and eq 2, for **3**(H_2O), with $x = J/k_BT$ and t the temperature-independent paramagnetism. g was fixed to 2 in the calculations.

$$\chi_m T \approx \frac{\mathscr{M}}{nH} T = 2\frac{N_A\beta_e^2}{k_B T} g^2 \times \frac{\exp(2x) + 5\exp(6x) + 14\exp(12x) + 30\exp(20x) + 55\exp(30x)}{1 + 3\exp(2x) + 5\exp(6x) + 7\exp(12x) + 9\exp(20x) + 11\exp(30x)} + 2tT \quad (1)$$

$$\chi_m T \approx \frac{\mathscr{M}}{nH} T = \frac{1}{4}\frac{N_A\beta_e^2}{k_B T} g^2 \frac{1 + 10\exp(3x) + 35\exp(8x) + 84\exp(15x) + 165\exp(24x)}{1 + 2\exp(3x) + 3\exp(8x) + 4\exp(15x) + 5\exp(24x)} + 2tT \quad (2)$$

Electrochemistry. Cyclic voltammetric studies (E_{pa}, anodic peak potential; E_{pc}, cathodic peak potential; $E_{1/2} = (E_{pa} + E_{pc})/2$; $\Delta E_p = E_{pa} - E_{pc}$) and exhaustive electrolyses were run under an argon atmosphere in a glovebox, using a standard three-electrode electrochemical cell. All potentials are referred to a Ag/10 mM Ag^+ reference electrode in acetonitrile + tetra-*n*-butylammonium perchlorate (TBAP) electrolyte and can be converted to the normal hydrogen electrode (NHE) by adding 0.52 V. The potential of the regular ferrocene/ferrocinium (Fc/Fc^+) redox couple used as an internal standard was 0.07 V under our experimental conditions. The working electrode was a platinum disk (0.2 cm^2) polished with 1 μm diamond paste. Exhaustive electrolyses were carried out with a carbon felt electrode (RCV 2000, 65 mg cm^{-3}, from Le Carbone Lorraine). The electrolyte was a 0.1 M solution of supporting electrolyte in CH_3CN (Rathburn, HPLC grade S). TBAP was obtained from Fluka (puriss) and stored under argon. Electrochemical measurements were carried out using an EG&G PAR model 173 potenstiostat equipped with a model 179 digital coulometer and a model 175 programmer with output recorded on a Sefram TGM 164 X-Y recorder.

Results

Syntheses. Reaction of HL with Mn^{2+} salts in methanol affords the dimanganese(II) complexes **1**·L and **2**·L (L = H_2O or CH_3OH) while that with Mn^{3+} affords the dimanganese(II,III) compound **3**(H_2O). It thus appears that the dimanganese(III,III) compound is not stable and that one Mn^{III} ion has been reduced, possibly by the solvent methanol, giving rise to the mixed-valent $Mn^{II}Mn^{III}$ state which is quite stable in aerobic conditions. The nature of the exogeneous ligand L may vary with the reaction and crystallization conditions pointing to a facile ligand exchange on this position. Therefore, it is likely that in acetonitrile solution the solvent molecule replaces the exogeneous water or methanol molecule (see below). Complexes **1**−**3** have been characterized by elemental analyses and shown to have the proposed formula. Electrospray ionization mass spectrometry (ESI-MS) analyses confirmed the nature of the cation after loss of the methanol (**1**) and the water (**2** and **3**) molecules.

(59) Sheldrick, G. M. *SHELXTL-Plus*, 5th ed.; Sheldrick, G. M., Ed.; University of Göttingen: Göttingen, Germany, 1994.
(60) Kahn, O. *Molecular Magnetism*; VCH: New York, 1993.

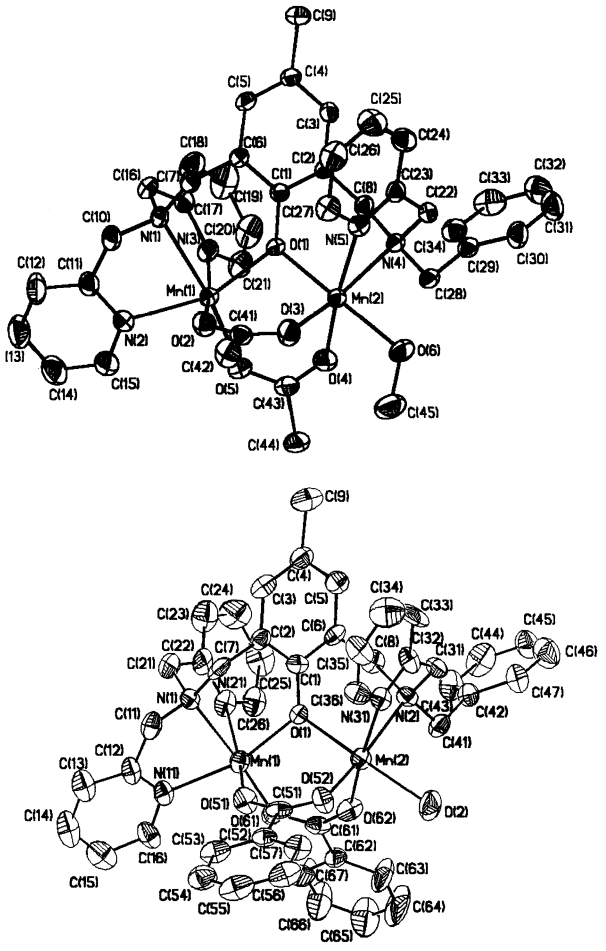

Figure 1. Structures of the cation $[Mn_2(\mu\text{-L})(\mu\text{-OAc})_2(CH_3OH)]^+$ (top) and of the cation $[Mn_2(\mu\text{-L})(\mu\text{-OBz})_2(H_2O)]^+$ (bottom). Ellipsoids are drawn at 30% probability.

In the case of **3**, it is worth noting that ESI-MS in the positive mode leads to the detection of the cation of **1** due to reduction of the $Mn^{II}Mn^{III}$ center in the spectrometer. By contrast, in the negative mode several ions derived from **3** can be observed. Infrared spectroscopy confirmed the presence of carboxylate ligands. Indeed, for the three compounds **1**−**3**, the antisymmetric vibration ν_{asCOO} was found at ca. 1600 cm^{-1} (1594, 1602, and 1601 cm^{-1}, respectively) and the symmetric one ν_{sCOO} near 1400 cm^{-1} (1434, 1399, and 1433 cm^{-1}, respectively). In all cases the splitting of the two bands (160, 203, and 168 cm^{-1}, respectively) suggests that the carboxylate ligands adopt the bridging mode.[61] In addition, the vibrations of uncoordinated perchlorates are noted near 1100 cm^{-1}.

X-ray Structure Determinations. Dimanganese(II) Complexes. Crystals of the acetate and benzoate complexes, **1**(CH_3OH) and **2**(H_2O), respectively, have been obtained from methanol solutions. Table 1 summarizes the relevant crystal data. Both compounds appear as a monocation with a noncoordinated perchlorate counterion. The structures of the cations are illustrated in Figure 1, and important bond lengths are summarized in Table 2. In both cases, the two Mn ions are triply bridged by the phenolate and two $\mu_{1,3}$-carboxylates. The coordination of Mn(1) is completed by the three nitrogen atoms of the bis(picolyl)amine branch of the ligand while that of Mn(2) is completed by the two nitrogen atoms of the benzylpicolylamine branch and an oxygen atom from an exogeneous ligand, methanol for **1**(CH_3OH) and water for **2**(H_2O). Both Mn atoms are in a slightly distorted octahedral environment. A perusal of Table 2 reveals that in **1**(CH_3OH) the coordination of the Mn atoms is less distorted than in **2**(H_2O) and also that the two Mn atoms are more similar. The distances between the Mn atoms and the bridging phenoxo oxygen (2.07−2.12 Å) and the corresponding Mn−O−Mn angles (ca. 109°) are close to those observed (2.10 Å and 107°, respectively) in the Mn^{II}_2 complex of a heptadentate phenol with two bis(methoxyethyl)amine groups[50] and slightly different from complexes of pentadentate phenols with two aminoalkylimine groups (2.121−2.214 Å and 94−110°, respectively).[43,46−48] The Mn−Mn distances (ca 3.43 Å) are in the range expected from literature data (3.33−3.60 Å). The Mn−N and Mn−O(carboxylate) bond lengths are in the ranges 2.18−2.37 and 2.04−2.20 Å, respectively, in agreement with literature data. The Mn−O bond lengths with the exogeneous solvent are close to 2.25 Å.

Dimanganese(II,III) Complexes. Crystals of the mixed-valent complex **3**(H_2O) were grown from methanol solutions. Crystal data are summarized in Table 1. As shown in Figure 2, **3**(H_2O) appears as a dication with two uncoordinated perchlorate counterions. The two Mn ions are triply bridged by the phenolate and the two $\mu_{1,3}$-carboxylates. The coordination of Mn(1) is completed by the three nitrogen atoms of the bis(picolyl)amine branch while that of Mn(2) is completed by the two nitrogen atoms of the benzylpicolylamine branch and an oxygen atom from an exogeneous water. Both Mn atoms are in a slightly distorted octahedral environment.

Examination of Table 2, which summarizes important bond lengths, shows that all distances from Mn(1) to donor atoms are significantly shorter than those from Mn(2). Indeed, these distances average to 2.049 Å vs 2.200 Å, respectively. This observation leads to conclude that the valences of the two ions are localized and that Mn(1) is the Mn^{III} ion. This conclusion is supported by two observations. First, the coordination sphere of Mn(2) is much less distorted than that of Mn(1). Indeed, for Mn(2) the sums of the bond distances along the three main axes ($\Sigma_{x,y,z}$ in Table 2) differ by 0.081 Å. This value is close to the range 0.091−0.159 Å observed for **1**(CH_3OH) and **2**(H_2O). For Mn(1) in **3**(H_2O), on the contrary, these sums differ by 0.355 Å. This enhanced geometrical distortion of Mn(1) results from the Jahn−Teller effect associated with the Mn^{III} ion. Careful examination of these parameters shows that in **3**(H_2O) Mn(1) is rhombically distorted. Second, the coordination of the Mn(2) ion is very similar to those of the Mn ions in **1**(CH_3OH) and **2**(H_2O). Indeed, the Mn−donor atom distances average 2.215, 2.206, 2.177, and 2.200 Å in these compounds and 2.200 Å for Mn(2). Interestingly, this similarity holds for all individual distances but the Mn−O(phenoxo) bond length which is longer in **3**(H_2O), 2.24 Å vs 2.1 Å in **1**(CH_3OH) and **2**(H_2O),

(61) Nakamoto, K. *Infrared and Raman spectra of inorganic and coordination compounds*, 5th ed.; Wiley-Interscience: New York, 1997; Part B, p 60.

Table 2. Important Bond Distances around the Manganese Atoms in Complexes **1**−**3**[a]

	1(CH_3OH)		**2**(H_2O)		**3**(H_2O)	
	Mn1	Mn2	Mn1	Mn2	Mn1	Mn2
d_{Mn-Mn} (Å)	3.423		3.445		3.497	
$\angle_{Mn-O-Mn}$ (deg)	108.70(3)		110.6(3)		115.59(7)	
			Distances (Å)			
Mn−O(phen)	2.1067(7)	2.1052(7)	2.074(6)	2.116(7)	1.8727(14)	2.2448(16)
Mn−N(tert)	2.3343(8)	2.3506(8)	2.293(8)	2.370(8)	2.130(2)	2.3528(18)
Mn−N(py-trans)	2.2716(9)		2.211(9)		2.0503(19)	
Mn−N(py-cis)	2.2966(9)	2.2897(9)	2.304(10)	2.243(9)	2.2207(19)	2.2369(18)
Mn−O(carb-trans)	2.1075(8)	2.1148(8)	2.049(7)	2.097(8)	1.9609(16)	2.0955(16)
Mn−O(carb-cis)	2.1722(8)	2.1402(9)	2.130(9)	2.113(9)	2.0569(16)	2.1302(15)
Mn−O(exogeneous)		2.2381(8)		2.259(8)		2.143(2)
Σ_x	4.4688	4.4299	4.434	4.340	4.2776	4.3671
Σ_y(Mn−N_{tert})	4.4410	4.4654	4.342	4.483	4.0909	4.4483
Σ_z(Mn−O_{phen})	4.3783	4.3433	4.285	4.375	3.923	4.3878
⟨Mn−O/N⟩	2.2148	2.2064	2.177	2.200	2.049	2.200

[a] O(phen): bridging phenolate. N(tert): tertiary nitrogen. N(py-trans): pyridine N trans to the phenolate. N(py-cis): pyridine N cis to the phenolate. O(carb-trans): carboxylate O trans to the tertiary N. O(carb-cis): carboxylate O cis to the tertiary N. O(exogeneous): O from the exogeneous water or methanol. Σ: sum of Mn−ligand distances on the same axis. ⟨Mn−O/N⟩: mean Mn−ligand distance.

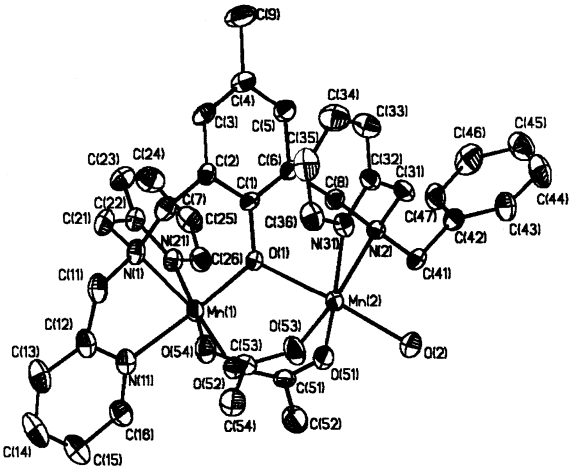

Figure 2. Structure of the cation $[Mn_2(\mu\text{-L})(\mu\text{-OAc})_2(H_2O)]^{2+}$. Ellipsoids are drawn at 30% probability.

and the Mn−O(methanol or water) bond length which is shorter in **3**(H_2O), 2.16 Å vs ca. 2.25 Å in **1**(CH_3OH) and **2**(H_2O). These differences in the bond lengths reflect the change in the oxidation state of Mn(1) (see below). The Mn−Mn distances (ca. 3.50 Å) and the Mn−O−Mn angles (115.6°) are in the range expected from literature data (3.44−3.54 Å and 114−117°, respectively).[42,52−54] The Mn−N and Mn−O bond lengths are in the ranges expected from literature for both the Mn^{II} and the Mn^{III} ions.

Magnetism. The magnetic properties of compounds **1**−**3** have been investigated over the temperature range 5−300 K at 0.5 and 5 T. No significant field dependence of the magnetic susceptibility (χ_m) was observed. The temperature dependence of the product of the molar magnetic susceptibility by temperature at 0.5 T of complex **1**(CH_3OH) is illustrated in Figure 3. $\chi_m T$ decreases smoothly from 8 $cm^3 \cdot K \cdot mol^{-1}$ at 300 K to 6 $cm^3 \cdot K \cdot mol^{-1}$ at 100 K and then more abruptly to reach 0.24 $cm^3 \cdot K \cdot mol^{-1}$ at 5 K. Complex **2**(H_2O) exhibits a very similar behavior. This behavior is characteristic of two high-spin ($S = 5/2$) Mn^{II} ions experiencing a moderate antiferromagnetic coupling. The magnetic data for **1**(CH_3OH) and **2**(H_2O) could be accounted for by using the Van Vleck equation for two spins $S = 5/2$ (see

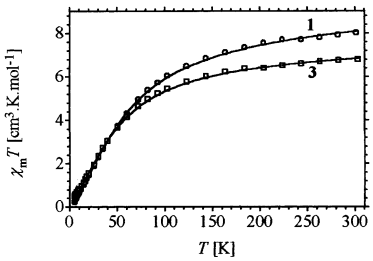

Figure 3. Temperature dependence of the $\chi_m T$ product for microcrystalline samples of **1** (○) and **3** (□). The experimental data were collected at 0.5 T and corrected for the diamagnetic contribution. The solid lines represent the curves calculated with the best least-squares fit parameters: for **1**, $-J = 4.28$ cm^{-1}, $t = 633 \times 10^{-6}$ $cm^3 \cdot mol^{-1}$; for **3**, $-J = 4.33$ cm^{-1}, $t = 315 \times 10^{-6}$ $cm^3 \cdot mol^{-1}$.

Experimental Section for details of the fitting procedure). The best least-squares fits of the experimental data were obtained with the following sets of parameters: for **1**(CH_3OH), $-J = 4.3(1)$ cm^{-1}, $t = 6(1) \times 10^{-4}$ $cm^3 \cdot mol^{-1}$; for **2**(H_2O), $-J = 4.4(1)$ cm^{-1}, $t = 2.36(5) \times 10^{-4}$ $cm^3 \cdot mol^{-1}$.

The temperature dependence of the product of the molar magnetic susceptibility by temperature of the mixed-valent complex **3**(H_2O) is illustrated in Figure 3. $\chi_m T$ decreases smoothly from 6.8 $cm^3 \cdot K \cdot mol^{-1}$ at 300 K to 5 $cm^3 \cdot K \cdot mol^{-1}$ at 80 K and then more steeply to reach 0.5 $cm^3 \cdot K \cdot mol^{-1}$ at 5 K. Such a behavior is consistent with what is expected for two moderately antiferromagnetically coupled spins $S = 5/2$ (Mn^{II}) and $S = 2$ (Mn^{III}). In this case, the Van Vleck equation, based on the magnetic exchange Heisenberg Hamiltonian, is not strictly valid because the zero-field splitting parameter D of the Mn^{III} ion can be of the same order of magnitude as the magnetic exchange interaction J. Nevertheless, the absence of any significant field dependence of the magnetic susceptbility indicates that D must be small. As already observed in the literature, the use of the VanVleck equation allows the experimental data to be satisfactorily simulated. The best least-squares fit, shown in Figure 3b, was obtained with the following parameters: $-J = 4.3(1)$ cm^{-1}; $t = 3(1) \times 10^{-4}$ $cm^3 \cdot mol^{-1}$.

The exchange interactions evaluated for **1**−**3** are very similar despite the difference in oxidation state of the Mn pair. They appear in the medium range of the domain

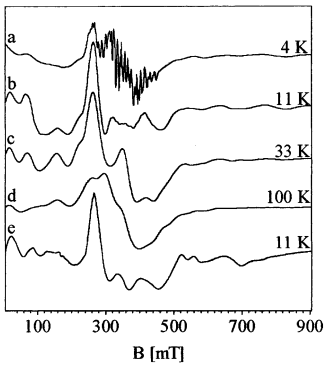

Figure 4. EPR spectra of $[Mn_2(L)(OAc)_2(CH_3OH)](ClO_4)$: (a−d) as a polycrystalline sample at 4, 11, 33, and 100 K, respectively, microwave frequency of 9.66 GHz, microwave power of 12.6 mW, modulation frequency of 100 kHz, modulation amplitude of 1.04 mT, and one scan for 168 s; (e) in acetonitrile solution at 11 K, microwave frequency of 9.6612 GHz, microwave power of 3.17 mW, modulation frequency of 100 kHz, modulation amplitude of 0.9 mT, and one scan for 168 s.

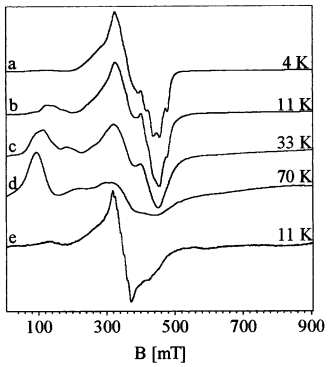

Figure 5. EPR spectra of $[Mn_2(L)(OAc)_2(H_2O)](ClO_4)_2$: (a−d) as a polycrystalline sample at 4, 11, 33, and 70 K respectively, microwave frequency of 9.659 GHz, microwave power of 3.16 mW, modulation frequency of 100 kHz, modulation amplitude of 1.04 mT, one scan for 168 s, and intensity multiplied by temperature to see small lines; (e) in acetonitrile solution at 11 K, microwave frequency of 9.6528 GHz, microwave power of 3.17 mW, modulation frequency of 100 kHz, modulation amplitude of 0.9 mT, and one scan for 336 s.

spanned by these kinds of complexes which extend from −2 to −8 cm^{-1}.[42,43,45−48,50,53,62] Although this domain is rather narrow, a tentative magneto−structural correlations can be elaborated from these data for the two series of compounds (see below).

EPR Spectroscopy. The EPR properties of compounds **1**−**3** have been investigated both in the polycrystalline state and in solution. Figure 4a−d illustrates the temperature dependence of the unsaturated EPR spectra of polycrystalline **1**(CH_3OH). Similar spectra and behavior are observed in frozen solution. Figure 4e shows the EPR spectrum of **1**(CH_3-OH) in acetonitrile, which is quite similar to the powder spectrum b. This indicates that the solid-state structure is conserved in acetonitrile solution. At 4 K the spectrum extends over at least 900 mT. The absorption in the 270−460 mT region exhibits a complex multiline pattern with ca. 21 lines. The value of this hyperfine splitting ca 8.8 mT, and the ca. 21 lines (line width ca. 3 mT) indicate that it is due to a dimanganese(II,III) center.[63] The small intensity of this signal indicates that this oxidation state is an impurity. The multiline feature in the 241−293 mT region (more easily seen on the derivative of spectrum e in solution as shown in Figure S1) exhibiting 11 lines with an hyperfine splitting of ca. 4.4 mT is characteristic of a dimanganese(II) center.[40,43,64] At 4 K, for $-J = 4.3$ cm^{-1}, $S = 1$ is almost the only populated EPR-active spin state. Thus, the weak and broad signal extending over at least 900 mT with the peak at ca. 265 mT could be associated to the $S = 1$ spin state. At 11 K, the hyperfine structure of the dimanganese(II,III) species disappears, new broad lines appear as the result of the population of higher excited spin states of the dimanganese-(II) center, and the 11 lines are still visible in solution on the top of the more intense peak at ca. 265 mT. As expected, the intensity of the broad signal extending over at least 900 mT increased (as roughly showed by the height of the peak at ca. 265 mT for example, which increased by a factor of 2.2 compared to the theoretical factor 3.8) and the spectrum associated with $S = 2$ should be present. At 33 K, the $S = 1$ spectrum decreased (the height of the peak at ca. 265 mT decreased by a factor of 1.3 compared to 1.2 theoretically) but the $S = 2$ spectrum should still increase. New lines appeared corresponding to spin states higher than $S = 1$. At 100 K, both spectra associated with $S = 1$ and $S = 2$ decrease, by a factor 2.0 for $S = 1$ (a factor 2.6 was measured at ca. 265 mT). The attribution of the 4 K signal to the $S = 1$ spin state is thus confirmed. This attribution contrasts with that proposed for other species where the low-temperature EPR signal is attributed to the $S = 2$ spin state in agreement with their smaller antiferromagnetic coupling ($-J = 1-2$ cm^{-1} *vs* 4 cm^{-1}).[65,66]

Figure 5 illustrates the spectrum of **3**(H_2O) both in the polycrystalline state over the temperature range 4−70 K (spectra a−d) and in an acetonitrile solution at 11 K (spectrum e). These spectra exhibit two components. One is near $g = 2$ (200−520 mT) which dominates the spectrum at low temperature and is therefore associated with the ground spin state $S = {}^1/_2$. It saturates slightly at 12.6 mW. When the temperature is increased, this feature loses intensity while an absorption feature near $g = 6$ (between $g = 3.9$ and $g = 8$) becomes dominant. These lines are associated with the first and next excited spin states $S = 3/2$, 5/2, 7/2, and 9/2. This behavior and shape corresponds to a dimanganese(II,-III) species. The same behavior and shape of spectra were already observed in two other dimanganese(II,III) complexes.[53,62] The spectrum of **3** in solution presents the same shape and behavior, except for the presence of a second species with an intensity depending on the solvent. It can be easily observed in acetonitrile (Figure 5e) and is characterized by six weak hyperfine splittings (9.1 mT) near $g =$

(62) Buchanan, R. M.; Oberhausen, K. J.; Richardson, J. F. *Inorg. Chem.* **1988**, *27*, 971−973.
(63) Khangulov, S.; Barynin, V. V.; Voyevodskaya, N.; Grebenko, A. *Biochim. Biophys. Acta* **1990**, *1020*, 305−310.
(64) Khangulov, S.; Pessiki, P.; Barynin, V.; Ash, D.; Dismukes, G. *Biochemistry* **1995**, *34*, 2015−2025.
(65) Howard, T.; Telser, J.; DeRose, V. *Inorg. Chem.* **2000**, *39*, 3379−3385.
(66) Le Pape, L.; Perret, E.; Michaud-Soret, I.; Latour, J. M. *JBIC* **2002**, *7*, 445−450.

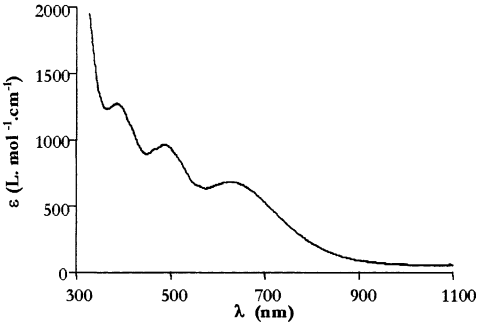

Figure 6. UV−visible spectrum of **3** in acetonitrile.

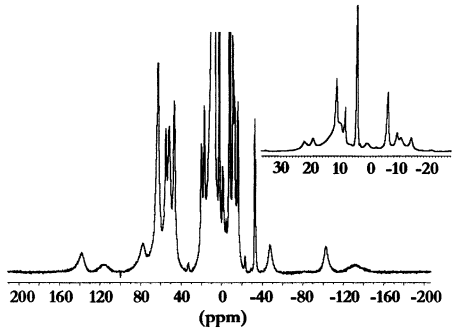

Figure 7. NMR spectrum of **3** in deuterated acetonitrile at 20 °C.

2 (extrema at 318 and 371 mT) (Figure 5e). Their probable origin lies in the disruption of the phenolate bridge through its protonation by residual water of the solvent.[41,67]

UV−Visible Spectroscopy. As shown in Figure 6 the mixed-valent complex **3**(H_2O) exhibits in acetonitrile moderately intense absorptions in the visible region at 627 nm ($\epsilon = 680$ L·mol^{-1}·cm^{-1}), 485 nm ($\epsilon = 960$ L·mol^{-1}·cm^{-1}), and 380 nm ($\epsilon = 1270$ L·mol^{-1}·cm^{-1}). Both the energy and the intensity of these absorptions match those of related complexes of the tetrapyridyl[53] and tetraimidazole ligands.[62] The most intense absorption at higher energy corresponds probably to a phenoxo to Mn^{III} charge-transfer transition while the less intense other two may be associated to d−d transitions of the Mn^{III} ion.[68]

^{1}H NMR Spectroscopy. As shown in Figure 7 the NMR spectrum of **3**(H_2O) extends over 270 ppm. A very wide spectral range of ca. 600 ppm was observed also for the mixed-valent diiron complexes of the present unsymmetrical ligand.[57] Nevertheless, comparison of the analogous Mn^{II}-Mn^{III} and $Fe^{II}Fe^{III}$ complexes of the present ligand reveals very different behaviors since the spectral width is three times larger in the diiron compound, a feature not anticipated from their rather similar magnetic properties ($\mu_{eff}^2 = 58\ \mu_B^2$ and $-J = 3.2$ cm^{-1} for the diiron complex vs 52.8 μ_B^2 and 4.3 cm^{-1}, respectively, for **3**(H_2O)). This discrepancy was not observed in NMR studies of μ-oxo $Mn^{III}Mn^{III}$ complexes.[69−72]

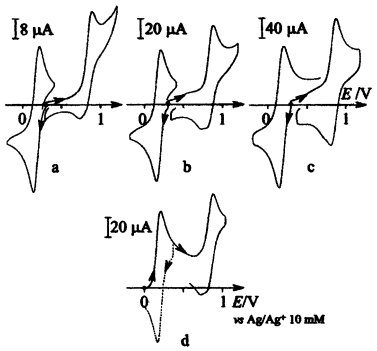

Figure 8. Cyclic voltamograms at a Pt electrode (diameter 5 mm) in acetonitrile + 0.1 M TBAP of **3** (1.1 mM) at different sweep rates: (a) 20 mV·s^{-1}; (b) 100 mV·s^{-1}; (c) 500 mV·s^{-1}; (d) after exhaustive reduction at 0.00 V with a sweep rate of 100 mV·s^{-1}.

Indeed they showed a close correspondence between the magnetic properties and the NMR peak position, and this was strongly indicative of the dominence of the contact contribution to the hyperfine shifts.[72] By contrast, the difference observed in this study suggests that dipolar effects may play a stronger role in **3**(H_2O) and the related diiron complexes.

Electrochemistry. The electrochemical properties of complexes **1**−**3** have been studied at a Pt electrode in acetonitrile with tetrabutylammonium perchlorate as supporting electrolyte. Figure 8 presents the cyclic voltammograms recorded for complex **3**(H_2O) at different sweep rates. At all sweep rates investigated in the range 20−500 mV·s^{-1}, the cyclic voltammograms of **3**(H_2O) exhibit a reversible reduction wave at $E_{1/2} = 0.18$ V vs Ag/Ag$^+$ (10 mM) ($\Delta E_p = 0.06$ V, $I_{pa}/I_{pc} = 0.9$) corresponding to the Mn^{II}_2/Mn^{II}-Mn^{III} redox couple. This potential is independent of the sweep rate. Exhaustive electrolysis at a potential of 0.00 V of the solution requires 0.95 electron/molecule of **3**(H_2O) indicating a one-electron process. The reduced Mn^{II}_2 species is obtained with a 95% yield as attested by the cyclic voltammogram of the resulting solution (Figure 8d). On the oxidative side, **3**(H_2O) exhibits a peak at $E_{pa} = 0.91$ V, assigned to the formation of a Mn^{III}_2 species, to which are associated at 100 mV·s^{-1} (Figure 8b) two reduction peaks at $E_{pc1} = 0.79$ V and $E_{pc2} = 0.71$ V. When the sweep rate is decreased to 20 mV·s^{-1} (Figure 8a), the latter peak maximizes at the expense of the former, while the reverse occurs at 500 mV·s^{-1} (Figure 8c). Such a behavior indicates that a chemical reaction is following the oxidative electron transfer (EC mechanism) and that the rate of this reaction is of the same order of magnitude as that of the electron transfer. An exhaustive electrolysis of a solution of **3**(H_2O) at 0.95 V consumes more than 3 electrons/molecule of **3**(H_2O) and leads to an irreversible transformation of the complex, showing the unstability of the Mn^{III}_2 species. Owing to the oxophilicity of the Mn^{III} ion, it is likely that a reaction with residual water occurs leading to the formation of an oxodimanganese(III) species which can be further oxidized to higher valent dioxo

(67) Dubois, L.; Caspar, R.; Jacquamet, L.; Petit, P. E.; Charlot, M. F.; Baffert, C.; Collomb, M. N.; Deronzier, A.; Latour, J. M. Manuscript in preparation.
(68) Vincent, J. B.; Folting, K.; Huffman, J. C.; Christou, G. *Inorg. Chem.* **1986**, *25*, 996−999.
(69) Sheats, J. E.; Czernuszewicz, R. S.; Dismukes, G. C.; Rheingold, A. L.; Petrouleas, V.; Stubbe, J.; Armstrong, W.; Beer, R. H.; Lippard, S. J. *J. Am. Chem. Soc.* **1987**, *109*, 1435−1444.
(70) Bonadies, J. A.; Maroney, M. J.; Pecoraro, V. L. *Inorg. Chem.* **1989**, *28*, 2044−2051.
(71) Hage, R.; Gunnewegh, E. A.; Niel, J.; Tsjan, F. S. B.; Weyermuller, T.; Wieghardt, K. *Inorg. Chim. Acta* **1998**, *268*, 43−48.
(72) Wright, D.; Mok, H. J.; Dubé, C. E.; Armstrong, W. H. *Inorg. Chem.* **1998**, *37*, 3714−3718.

species. It is noteworthy that mono- and dioxo derivatives are formed upon reaction of **1**(CH_3OH) with H_2O_2.[67] On the other hand, **1**(CH_3OH) gives a cyclic voltammogram identical to that of the one-electron-reduced form of **3**(H_2O) (Figure 8d) and the one-electron-oxidized form of **1**(CH_3OH) gives a cyclic voltammogram identical to that of **3**(H_2O). These observations suggest that, upon dissolution in acetonitrile, the exogeneous ligands are displaced by the solvent. In the case of **2**(H_2O), the two oxidative one-electron transfers assigned to the $Mn^{II}{}_2/Mn^{II}Mn^{III}$ and the $Mn^{II}Mn^{III}/Mn^{III}{}_2$ redox couples, respectively, are observed at $E_{1/2} = 0.24$ V and $E_{pa} = 1.01$ V. The one-electron oxidation forms of **1**(CH_3OH) and **2**(H_2O) are obtained by exhaustive oxidations 0.30 and 0.35 V, respectively.

Discussion

Solid-State Properties.

The present series of complexes differ from those derived from the usual tetrapyridyl[42,52,53] and tetraimidazole[62] phenolate ligands in that they provide an accessible coordination site on one manganese of the pair. The binding of a water/methanol has been documented by X-ray crystallography on the dimanganese(II) and -(II,III) compounds. Interestingly, the Mn−O bond lengths with the exogeneous solvent in the dimanganese(II) compounds **1**(CH_3OH) and **2**(H_2O) are close to 2.24 Å, shorter than the corresponding distance in the complex of a pentadentate phenol[48] (2.313 Å) and that of the chelating ether groups of the heptadentate phenol (2.27−2.32 Å),[50] indicating a strong interaction of the exogeneous ligand. This bond length is even shorter for **3**(H_2O), 2.16 Å, what can be explained in the following way. Replacement of the Mn^{II} in **1**(CH_3OH) and **2**(H_2O) by Mn^{III} in **3**(H_2O) strengthens the Mn(1)−O(1) bond making the phenolate oxygen less available. As a consequence, the Mn(2)−O(1) bond is weakened, and through a diminished trans effect, the bond between Mn(2) and the exogeneous ligand is strengthened. It appears, therefore, that the binding of this solvent molecule is sensitive to the oxidation state of the neighboring Mn ion which indicates a significant electronic communication between the two coordination sites.

Six (μ-phenoxo)bis(μ-carboxylato)dimanganese(II) complexes have been both structurally and magnetically characterized.[43,45−48,50] With the help of the results obtained for **1**(CH_3OH) and **2**(H_2O), the first rough magneto−structural correlation for these structurally related complexes can be tentatively established. If direct exchange and superexchange via carboxylate bridges are neglected, one can focus on the phenolate-bridge superexchange pathway. From the several possible parameters, the average distance between Mn and $O_{phenoxo}$ (d_{Mn-O}) appears essential. As expected, the general trend is a decrease of $-J$ as d_{Mn-O} increases (Figure 9). A linear regression gave the following equation:

$$-J = 50(10) - 20(5)d_{Mn-O} \quad (3)$$

Here J is expressed in cm^{-1} and d_{Mn-O} in Å. The large J-value difference observed at 2.15 Å could be due to a second parameter, the angle Mn−O−Mn, which is quite different between the two complexes: 101° ($-J = 4.0$ cm^{-1})[45] and 114° ($-J = 2.9$ cm^{-1}).[48] If d_{Mn-O} is fixed, $-J$ increases as this angle decreases.

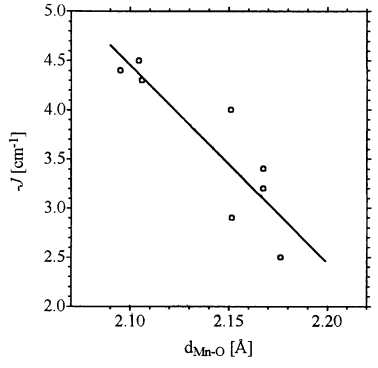

Figure 9. Magneto−structural correlation between $-J$ and d_{Mn-O} for (μ-phenoxo)bis(μ-carboxylato)dimanganese(II) complexes. Linear regression gave $-J = 46.8 - 20.2d_{Mn-O}$.

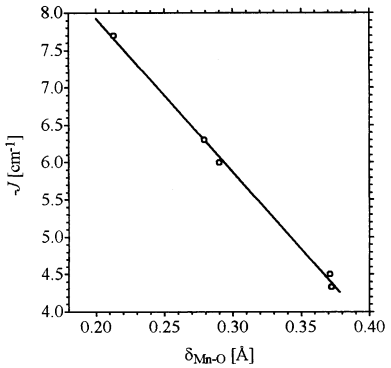

Figure 10. Magneto−structural correlation between $-J$ and δ_{Mn-O} for (μ-phenoxo)bis(μ-carboxylato)dimanganese(II,III) complexes. Linear regression gave $-J = 12.0 - 20.6\delta_{Mn-O}$.

Five (μ-phenoxo)bis(μ-carboxylato)dimanganese(II,III) complexes have been structurally and magnetically characterized.[42,46,53,62] The complex of the aminoalkylimino phenol ligand[46] has not been included as detailed below. Using **3**(H_2O) and these data a new magneto-structural correlation can be established. As for dimanganese(II), one can focus on the phenolate-bridge superexchange pathway. In contrast to the dimanganese(II) complexes, the Mn−O−Mn angles of the five compounds span a very limited range (112−117°) while the variations of the Mn^{II}−O and Mn^{III}−O distances are larger (2.13−2.26 and 1.87−1.96 Å, respectively). It has been suggested that the appreciable difference in Mn^{II}−O and Mn^{III}−O bond lengths (δ_{Mn-O}) could play a role in the magnetic interactions of these dimanganese(II,III) complexes.[53] Indeed, while rough correlations can be found between $-J$ and the respective Mn^{II}−O and Mn^{III}−O distances, a strict one exist with δ_{Mn-O} as illustrated in Figure 10 which shows the variation of $-J$ vs δ_{Mn-O}. A linear regression gave the following equation:

$$-J = 12.0(2) - 20.6(6)\delta_{Mn-O} \quad (4)$$

Here J is expressed in cm^{-1} and δ_{Mn-O} in Å.

The general trend is an increase of $-J$ as δ_{Mn-O} decreases. This $-J$ increase corresponds to a decrease in $d_{Mn(II)-O}$ as

Table 3. Electrochemical Data for (μ-Phenolato)bis(μ-carboxylato)dimanganese Complexes[a]

complex	$Mn^{II/II} \leftrightarrow Mn^{II/III}$	$Mn^{II/III} \leftrightarrow Mn^{III/III}$	ref
$[Mn_2(L)(\mu\text{-}OAc)_2(H_2O)](ClO_4)_2$, **3**($H_2O$)	$E_{1/2} = +0.70$ ($+0.18^b$) $\Delta E_p = 0.06$	$E_{pa} = +1.43$ ($+0.91^b$) $E_{pc1} = +1.31$ ($+0.79^b$) $E_{pc2} = +1.23$ ($+0.71^b$)	this work
$[Mn_2(L)(\mu\text{-}OBz)_2(H_2O)](ClO_4)$, **2**($H_2O$)	$E_{1/2} = +0.76$ ($+0.24^b$) $\Delta E_p = 0.16$	$E_{pa} = +1.53$($+1.01^b$) $E_{pc1} = +1.24$ ($+0.72^b$)	this work
$[Mn_2(bpmp)(\mu\text{-}OAc)_2](ClO_4)_2$	$E_{1/2} = +0.71$ ($+0.47^c$) $\Delta E_p = 0.12$	$E_{1/2} = +1.26$ ($+1.02^c$) $\Delta E_p = 0.17$	42
$[Mn_2(bpmp)(\mu\text{-}OBz)_2](ClO_4)_2$	$E_{1/2} = +0.77$ ($+0.53^c$) $\Delta E_p = 0.10$	$E_{1/2} = +1.31$ ($+1.07^c$) $\Delta E_p = 0.12$	42
$[Mn_2(L\text{-}Im)(\mu\text{-}OAc)_2](ClO_4)_2$	$E_{1/2} = +0.67$ ($+0.44^d$) $\Delta E_p = 0.12$	$E_{1/2} = +1.24$ ($+1.01^d$) $\Delta E_p = 0.18$	62

[a] Hbpmp: 2,6-(bis(2-pyridylmethyl)aminomethyl)-4-methylphenol. HL-Im: 2,6-(bis(2-imidazolylmethyl)aminomethyl)-4-methylphenol. [b−d] The values of the potentials reported in the literature are indicated in parentheses and have been converted to the normal hydrogen electrode with the following corrections: [b]$Ag/AgNO_3$ 10 mM ($\Delta E = +0.52$ V_{NHE}); [c]saturated calomel electrode ($\Delta E = +0.24$ V_{NHE}); [d]Ag/AgCl ($\Delta E = +0.23$ V_{NHE}).

expected from overlap considerations, but unexpectedly, it parallels an increase in the $Mn^{III}-O$ distance. This behavior can be explained by considering the Jahn−Teller distortions of the Mn^{III} coordination sphere. Indeed, for all complexes of the correlation the Jahn−Teller distortion can be described as a compression[62] along the $Mn^{III}-O_{phenoxo}$ axis or an elongation perpendicular to it[42,53] or gives rise to a highly rhombic Mn^{III} coordination sphere[53] as for **3**(H_2O). In all cases, the $Mn^{III}-O_{phenoxo}$ distance is the shortest and thus the z^2 orbital pointing toward the bridging phenoxo oxygen is the highest in energy: as a consequence, the shorter the $Mn^{III}-O$ distance, the lesser this orbital occupancy. As shown for dimanganese(III) complexes, this z^2 orbital is engaged in *crossed interactions* with the z^2, *xz*, and *yz* of the other ion and contributes antiferromagnetic interactions.[73] This explains why a shorter $Mn^{III}-O_{phenoxo}$ distance, which makes this orbital higher in energy and therefore less populated, is associated with a smaller value of $-J$. The importance of the Mn^{III} distortion on the magnetic exchange was initially observed for oxodimanganese(III) complexes.[74] In the present case, it is further supported by the fact that the only complex[46] which does not follow the correlation possesses a strikingly different Mn^{III} coordination. Indeed in this compound, the Jahn−Teller distortion is best described as an elongation along the $Mn^{III}-O_{phenoxo}$ axis and this orbital switching results from the presence of a strongly bound equatorial azide and from specific constraints brought by the iminophenol ligand.

Electrochemical Properties.

The presence of the exogeneous ligand confers specific electrochemical properties to complexes **1**−**3**. Table 3 summarizes the electrochemical properties of **2**(H_2O), **3**(H_2O), and a few complexes of tetraamino phenolate ligands. All potentials have been converted to the normal hydrogen electrode to facilitate comparison. The electrochemical potentials of the $Mn^{II}{}_2/Mn^{II}Mn^{III}$ couples of the acetato complexes are very similar and reflect the subtle differences in Mn ligation. Concerning the second oxidative electron transfer, assigned to the $Mn^{II}Mn^{III}/Mn^{III}{}_2$ couple, the present complexes differ from those of the tetraamino phenols in that they exhibit irreversible transfers at higher potentials. This irreversible transfer has been clearly evidenced for **3**(H_2O) (and **1**(CH_3OH)), where a chemical reaction has been shown to occur after the electron transfer. It is likely that this reaction involves a ligand substitution at the external Mn ion (Mn(2) in the crystal structures). Indeed, X-ray crystallography has shown that water or methanol can bind to this ion in the solid state. In acetonitrile solution, the identity of the cyclic voltammograms of **1**(CH_3OH) and **3**(H_2O) indicates that the solvent substitutes the H_2O or CH_3OH bound to the Mn^{II} in the $Mn^{II}{}_2$ and $Mn^{II}Mn^{III}$ centers of **1** and **3**, respectively. However, further oxidation of this center to the $Mn^{III}{}_2$ state makes the external Mn ion more acidic and therefore increases its affinity for oxygen ligands promoting acetonitrile substitution at this stage. Accordingly, the two peaks $E_{pc1} = 1.31$ V and $E_{pc2} = 1.23$ V vs NHE should correspond to reduction of the two species $[Mn_2(L)(OAc)_2(CH_3CN)]^{3+}$ and $[Mn_2(L)(OAc)_2(H_2O)]^{3+}$, respectively. Scheme 1 illustrates all electron transfers and associated ligand exchanges. A similar ligand exchange has been observed in the corresponding diiron complexes.[75] In that case, the ligand exchange rate was fast enough for a single reduction peak to be detected, the electrochemical potential of which depended on the water content of the acetonitrile solution. The benzoate complex **2**(H_2O) behaves as the acetate derivatives. In this respect, it is noteworthy that the 60 mV difference in the potentials of the $Mn^{II}{}_2/Mn^{II}Mn^{III}$ couple of the acetate and benzoate complexes is identical to that found for the same derivatives of the tetrapyridyl ligand (Table 3). It can thus be attributed to the influence of the carboxylate.

Examination of Table 3 reveals that the mixed-valent species in **3** has a larger stability domain than the analogous tetraamino phenolate complexes.[42] Indeed, the potential difference between the oxidative and the reductive electron transfers is larger by ca. 100 mV ($\Delta E = 670$ mV vs 540−570 mV). This translates into a hundred times larger comproportionation constant (2.1×10^{11} *vs* ca. 3×10^9) as shown in the following equation which relates the equilib-

(73) Hotzelmann, R.; Wieghardt, K.; Flörke, U.; Haupt, H. J.; Weatherburn, D. C.; Bonvoisin, J.; Blondin, G.; Girerd, J. J. *J. Am. Chem. Soc.* **1992**, *114*, 1681−1696.

(74) Corbella, M.; Costa, R.; Ribas, J.; Fries, P.; Latour, J.; Ohrstrom, L.; Solans, X.; Rodriguez, V. *Inorg. Chem.* **1996**, *35*, 1857−1865.

(75) Chardon-Noblat, S.; Deronzier, A.; Chabut, B.; Debaecker, N.; Jones, P.; Pécaut, J.; Avenier, F.; Dubois, L.; Jeandey, C.; Oddou, J. L.; Horner, O.; Latour, J. M. Manuscript in preparation.

Scheme 1

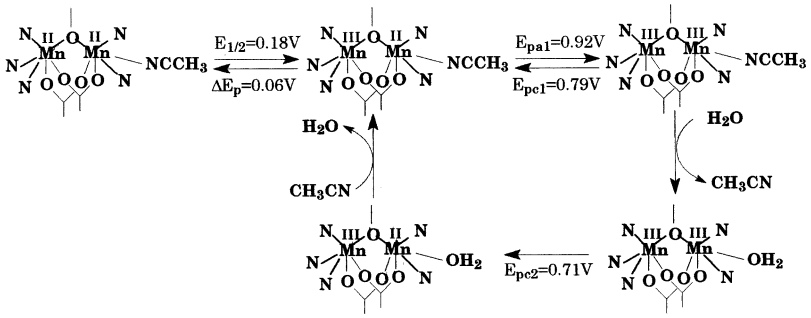

rium constant to the difference in oxidation and reduction potentials (N_3ON_2 represents the phenolate ligand L^-):

$$[Mn^{II}(N_3ON_2)Mn^{II}(S)]^+ + [Mn^{III}(N_3ON_2)Mn^{III}(S)]^{3+} \rightleftarrows [Mn^{III}(N_3ON_2)Mn^{II}(S)]^{2+} \quad (5)$$

$$\Delta E = (RT/nF) \ln K_{com} \quad S = CH_3CN$$

This difference does not originate in the reduction process since the potentials of the $Mn^{II}{}_2/Mn^{II}Mn^{III}$ couple are rather similar. This is indeed in line with the fact that the electroactive Mn ion is that located in the bis(picolyl)amine site. On the contrary, the $Mn^{II}Mn^{III}/Mn^{III}{}_2$ couple involves the Mn ion accessible to solvents and its potential is higher in the present case (1.37 *vs* 1.25(1) V). This ca. 100 mV difference can therefore be attributed to the binding of acetonitrile, a weaker donor and stronger acceptor than pyridine and imidazole. Gagné[76] has identified the various factors influencing the stability of mixed-valent forms of dinuclear metal compounds. These are (i) structural changes associated with the redox reactions, (ii) Coulombic interactions, (iii) magnetic exchange between the metal centers, and (iv) electronic delocalization which is expected to stabilize the mixed-valent form in **3**. In diiron complexes of the tetrapyridyl ligand, Que[77] estimated the latter factor to ca. 100 mV, but NMR experiments on diiron complexes of the present ligand showed that the valences are more localized in its complexes. Therefore, electron delocalization cannot be held responsible for the increased stability of the mixed-valent form. On the other hand, in the study of structurally related diiron compounds possessing a terminal phenolate on one iron of the pair, we showed that the asymmetry of the charge distribution was the major contributor to the enhanced stability of the mixed valent species.[57] This conclusion appears valid also in the case of the dimanganese complexes since a dimanganese complex of the same ligand with a terminal phenolate in place of the benzyl group exhibits a greatly enhanced stabilization of the mixed valent state (ΔE = 975 mV).[54] A similar but more moderate enhancement of the stability of the mixed-valent state is observed in the present complexes. Therefore, it can be attributed to the asymmetry of the electron density of the Mn pair introduced by the acetonitrile molecule.

Summary

In this article we have reported the syntheses and extensive structural, spectroscopic, magnetic, and redox characterization of dimanganese(II) and -(II,III) complexes of an unsymmetrical phenol-based ligand. In the solid state, the present compounds behave as similar complexes of the symmetrical phenolato ligands. This is further shown by the establishment of a magneto−structural correlation between the magnetic exchange interaction and the $Mn^{II}-O_{phenoxo}$ bond length for the dimanganese(II) complexes. For the dimanganese(II,III) complexes we showed that the magnetic exchange interaction is correlated with the difference between the two $Mn-O_{phenoxo}$ distances and is directly related to the Jahn−Teller distortion of the Mn^{III} ion.

On the other hand, the presence of an exogeneous ligand on one Mn ion of the pair gives rise to peculiar redox properties. First, a ligand exchange can be oxidatively induced. Second, the unsymmetry of the coordination of the Mn pair gives rise to an increased stability domain of the mixed-valent state. In this respect, it is of interest to note that the X-ray structure determinations of the Mn catalases[26,27] have revealed that their active site is rather symmetrical involving the same terminal ligands (histidine and glutamate) for the two Mn ions. Such an environment is not suited to stabilizing the dimanganese(II,III) mixed-valent form. This is quite consistent with their redox activity, which is based on shuttling between the dimanganese(II) and dimanganese(III) states[28] so as to avoid the deleterious one-electron reduction of hydrogen peroxide. The easy substitution of the exogenenous ligand in the present complexes has been used to study their reactivity with hydrogen peroxide, and the corresponding kinetic, thermodynamic, and mechanistic studies will be reported shortly.

Acknowledgment. This research was supported in part by the COST D21 program.

Supporting Information Available: X-ray crystallographic details (refined positional coordinates, anisotropic thermal parameters, complete bond lengths and angles) for complexes **1**−**3** in table and CIF format and the second-derivative EPR spectrum of **1**(CH_3OH) (Figure S1). This material is available free of charge via the Internet at http://pubs.acs.org.

IC020354M

(76) Gagné, R. R.; Spiro, C. L.; Smith, T. J.; Hamann, C. A.; Thies, W. R.; Shiemke, A. K. *J. Am. Chem. Soc.* **1981**, *103*, 4073−4081.
(77) Borovik, A. S.; Papaefthymiou, V.; Taylor, L. F.; Anderson, O. P.; Que, L., Jr. *J. Am. Chem. Soc.* **1989**, *111*, 6183−6195.